Engineering Against Fatigue, University of Sheffield, March 1997

Prediction of Crack Growth under Variable-Amplitude Loading in Thin-Sheet 2024-T3 Aluminum Alloys

J. C. Newman, Jr.
NASA Langley Research Center
Hampton, Virginia, USA

ABSTRACT

The present paper is concerned with the application of a "plasticity-induced" crack closure model to study fatigue crack growth under various load histories. The model was based on the Dugdale model but modified to leave plastically deformed material in the wake of the advancing crack. The model was used to correlate crack growth rates under constant-amplitude loading and then used to predict crack growth under variable-amplitude and spectrum loading on thin-sheet 2024-T3 aluminum alloys. Predicted crack-opening stresses agreed well with test data from the literature. The crack-growth lives agreed within a factor of two for single and repeated spike overloads/underloads and within 20 percent for spectrum loading. Differences were attributed to fretting-product-debris-induced closure and three-dimensional affects not included in the model.

INTRODUCTION

In 1968, Elber observed that fatigue-crack surfaces contact under cyclic loading. This simple observation and the crack-closure concept (Elber 1971) began to explain many crack-growth characteristics. Since the discovery of plasticity-induced crack closure, other closure mechanisms have been identified, such as roughness- and oxide-induced closure. These developments have greatly improved our understanding of the complex interactions that occur during fatigue crack growth under variable-amplitude loading (see Schijve 1988). Several numerical models of plasticity-induced crack closure have been developed, during the last twenty years, to calculate crack-opening stresses under aircraft spectrum loading, such as FASTRAN (Newman 1981).

The objective of this paper is to apply the FASTRAN crack-closure model to correlate constant-amplitude crack-growth rate data on 2024-T3 aluminum alloys and to predict crack growth under variable-amplitude loading and a commercial transport wing spectrum. The model included the influence of "constraint" on the development of crack-tip plasticity and closure. The paper will demonstrate how constraint plays a leading role in crack growth under variable-amplitude loading. The types of tests that are necessary to obtain baseline crack-growth rate data to predict crack growth under spectrum loading are discussed. Comparisons are made between measured and calculated crack-opening stresses for crack growth under a single spike overload and an underload. Comparisons are also made between measured and predicted crack-length-against-cycles, and fatigue crack growth lives from an initial crack length to failure, for single and repeated spike overloads/underloads, and for an aircraft wing spectrum loading.

PLASTICITY-INDUCED CRACK-CLOSURE MODEL

The plasticity-induced crack-closure model was developed for a central through crack in a finite-width specimen subjected to remote applied stress. The model was based on the strip-yield model (Dugdale 1960) but modified to leave plastically deformed material in the wake of the crack. The details of the model are given elsewhere and will not be presented here (Newman 1981). One of the most important features of the model is the ability to model three-dimensional

constraint effects. A constraint factor, α, is used to elevate the flow stress ($\alpha\sigma_o$) at the crack tip to account for the influence of stress state. (The flow stress σ_o is the average between the yield stress and ultimate tensile strength.) For plane-stress conditions, α is equal to unity (original Dugdale model); and for simulated plane-strain conditions, α is equal to 3. Although the strip-yield model does not model the correct yield-zone pattern for plane-strain conditions, the model with a high constraint factor is able to produce crack-surface displacements and crack-opening stresses quite similar to those calculated from three-dimensional, elastic-plastic, finite-element analysis of crack growth and closure for finite-thickness plates.

Effective stress-intensity factor range

For most damage tolerance and durability analyses, linear-elastic fatigue-crack growth analyses have been found to be quite adequate. The linear-elastic effective stress-intensity factor range developed by Elber (1971) is given by

$$\Delta K_{eff} = (S_{max} - S'_o) \sqrt{(\pi c)}\ F(c/w) \qquad (1)$$

where S_{max} is the maximum stress, S'_o is the crack-opening stress and F is the boundary-correction factor.

Constant-amplitude loading

Newman (1984) developed crack-opening stress equations from the plasticity-induced crack-closure model for a middle-crack tension specimen subjected to constant-amplitude loading. Later, the model and equations were modified (Newman 1992a) to account for extreme crack-growth rates, such as those under high loads or proof testing. Equations were then fit to the results from the model which gave crack-opening stress (S'_o) as a function of stress ratio (R), maximum stress level (S_{max}/σ_o) and the constraint factor (α). These equations are used to correlate fatigue crack growth rate data on middle-crack and compact tension specimens.

Constraint effects

As a crack grows in a plate under cyclic loading (constant stress range), the plastic-zone size at the crack front increases. At low stress-intensity factor levels, plane-strain conditions should prevail but as the plastic-zone size becomes large compared to thickness, a loss of constraint is expected (see Newman et al. 1993). This constraint loss has been associated with the transition from flat-to-slant crack growth. Schijve (1967) has shown that the transition occurs at nearly the same crack-growth rate (or ΔK_{eff}) over a wide range in stress ratios for an aluminum alloy. This observation has been used to help select the constraint-loss regime. Newman (1992b) developed an expression to predict the transition from flat-to-slant crack growth and the ΔK_{eff} at transition is given by

$$(\Delta K_{eff})_T = 0.5\ \sigma_o \sqrt{B} \qquad (2)$$

The range of the constraint-loss regime, in terms of rate or ΔK_{eff}, is a function of thickness but this relation has yet to be developed. Trial-and-error methods are used to establish the range.

CONSTANT-AMPLITUDE LOADING

To make crack-growth predictions, ΔK_{eff} as a function of crack-growth rate must be obtained over the widest possible range in rates (from threshold to fracture), especially if spectrum load predictions are required. Under constant-amplitude loading, the only unknown in the analysis is

the constraint factor, α. The constraint factor is determined by finding (by trial-and-error) a value (or values) that will correlate the constant-amplitude crack-growth-rate data over a wide range in stress ratios, as shown by Newman (1984). In the following, the ΔK_{eff} -rate relation for two aluminum alloys will be presented and discussed. A detailed description will be given for only one material. The same procedures are used to establish the relationship for other materials.

Aluminum alloy 2024-T3

Crack-growth results from Hudson (1969), Phillips (1988) and Dubensky (1971) for 2024-T3 aluminum alloy sheet (B = 2.3 mm) are shown in Figure 1. This figure shows the elastic ΔK_{eff} plotted against crack-growth rate. The data collapsed into a narrow band for all stress ratios. Some large differences occurred at high R-ratios in the high-rate regime. These tests were conducted at extremely high stress levels (0.75 and 0.95 of the yield stress). Even elastic-plastic analyses were unable to collapse the data along a unique curve in this region. From a high-cycle fatigue standpoint, however, this discrepancy has very little influence on total life. But the elastic-plastic fracture criterion (Two-Parameter Fracture Criterion; see Newman 1976) used in the analysis (K_F = 267 MPa$\sqrt{m}$; m = 1) predicted failure very near to the vertical asymptotes of the test data, see the vertical dashed and dotted lines for R = 0.7 and 0.5 (at 0.75 and 0.95 of yield).

For these data, a constraint factor (α) of 2.0 was used for rates less than 1E-07 m/cycle and α equal to 1.0 was used for rates greater than 2.5E-06 m/cycle. For intermediate rates, α was varied linearly with the logarithm of crack-growth rate. The values of α and rate were selected by trial-and-error and from analyses of crack growth under spectrum loading (see Newman 1992b). For the 2024-T3 alloy sheet, $(\Delta K_{eff})_T$ = 10.2 MPa$\sqrt{m}$, a value which falls within the constraint-loss regime.

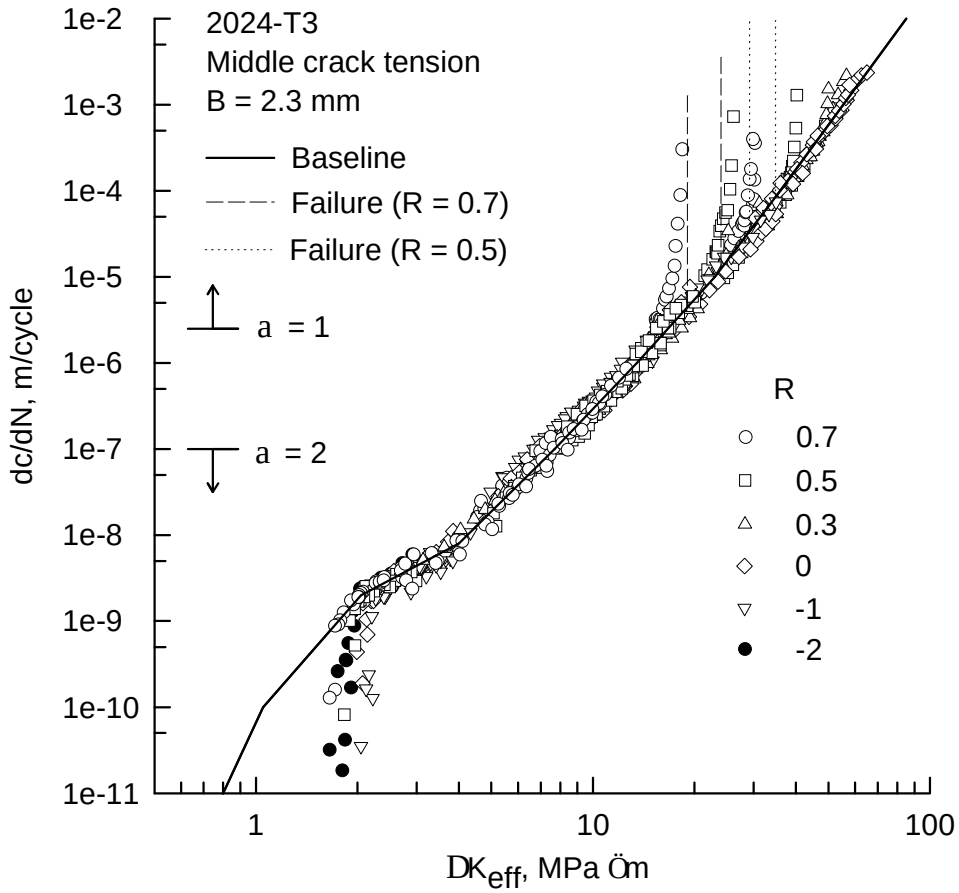

Figure 1 - Effective stress-intensity factor range against rate for 2024-T3 aluminum alloy sheet.

In the low crack-growth rate regime, near the large-crack threshold, tests and analyses have shown that thresholds develop because of a rise in the crack-opening-stresses due to the load-shedding procedure (see Newman 1983). In the threshold regime then, the actual ΔK_{eff} -rate data would lie at lower values of ΔK_{eff} because the rise in crack-opening stress was not accounted for in the current analysis. For the present study, an estimate was made for this behavior on the basis of small-crack data (Newman & Edwards 1988) and it is shown by the solid line below rates of about 2E-09 m/cycle. The baseline relation shown by the solid lines will be used later to predict crack growth under variable-amplitude and spectrum loading.

Aluminum alloy 2024-T351

Yisheng & Schijve (1995) made measurements of crack-opening stresses during a single-spike overload and underload for a 6.35 mm-thick aluminum alloy. In order to compare their measurements with the crack-closure model, a ΔK_{eff} -rate relation is needed for this alloy and thickness. Because the raw data at various R ratios was not available, a simple power-law relation was assumed as

$$dc/dN = C\,(\Delta K_{eff})^n \qquad (3)$$

The value of n was estimated to be 3.5 on the basis of other aluminum alloys and C = 3.9E-10 was determined by fitting to the constant amplitude portion of the crack length against cycles (before the overload and underload were applied), as shown in Figure 2. The constant-amplitude loading was S_{max} = 100 MPa at R = 0. For these data, a constraint factor (α) of 2.0 was used for

rates less than 1E-07 m/cycle but an α value of 1.2 was used for rates greater than 7E-06 m/cycle. The values of α and rate fall within the expected constraint-loss regime, $(\Delta K_{eff})_T = 17$ MPa$\sqrt{m}$, but their final values were selected on the basis of the spike overload tests. These types of tests seem to be more sensitive to the location of the constraint-loss regime and the selected values.

SINGLE-SPIKE OVERLOADS AND UNDERLOADS

Yisheng & Schijve (1995) conducted single-spike overload and underload tests on middle-crack tension specimens made of the 6.35 mm-thick aluminum alloy. In one test, a crack was grown from an initial size to 6 mm at $S_{max} = 100$ MPa and R = 0. At this point, a 200 MPa overload (S_{OL}) was applied and the test was continued at the previous constant-amplitude loading. In the second test, a crack was grown to 7.5 mm under the constant-amplitude loading and the same overload was applied but then an underload (S_{UL}) of -80 MPa was applied. The test was then continued at the previous constant-amplitude loading. During these tests, the crack length against cycles and crack-opening stresses were measured during and after the overload.

The measured crack length against cycles from these two tests are shown in Figure 2. (Note that the cycles have been shifted in order to get both results on the same plot.) These results show that the overload causes an immediate crack-growth delay and that the application of the underload, immediately after the overload, reduces some of the crack-growth delay caused by the overload. The solid curves show the calculated results using equation 3 and the closure model. The solid symbols show where the analyses have been anchored. The analyses are in reasonable agreement with the test data. But the analysis for the overload case tended to predict slower rates immediately after the overload than the test. The reason for this discrepancy is not known but may be related to three-dimensional effects due to crack tunneling and closure differences through the thickness (see Vlasveld & Schijve 1980). The closure model accurately predicted the reduction in crack-growth delay due to the compressive underload.

Figure 3 shows a comparison of measured and calculated crack-opening stresses for the single-overload test. The calculated results agreed reasonably well with the measured trends. The model tended to predict slightly higher opening stresses for the overload case but matched the overload/underload results very well (not shown), considering the scatter in the measured values. The length of influence of the overload in terms of cycles was predicted extremely well by the model. These test results and analyses occurred almost exclusively in the constraint-loss regime (α varied from 1.85 to 1.2). The saw-tooth nature of the calculated results are due to the lumping procedure to eliminate elements in the model to maintain model efficiency and speed.

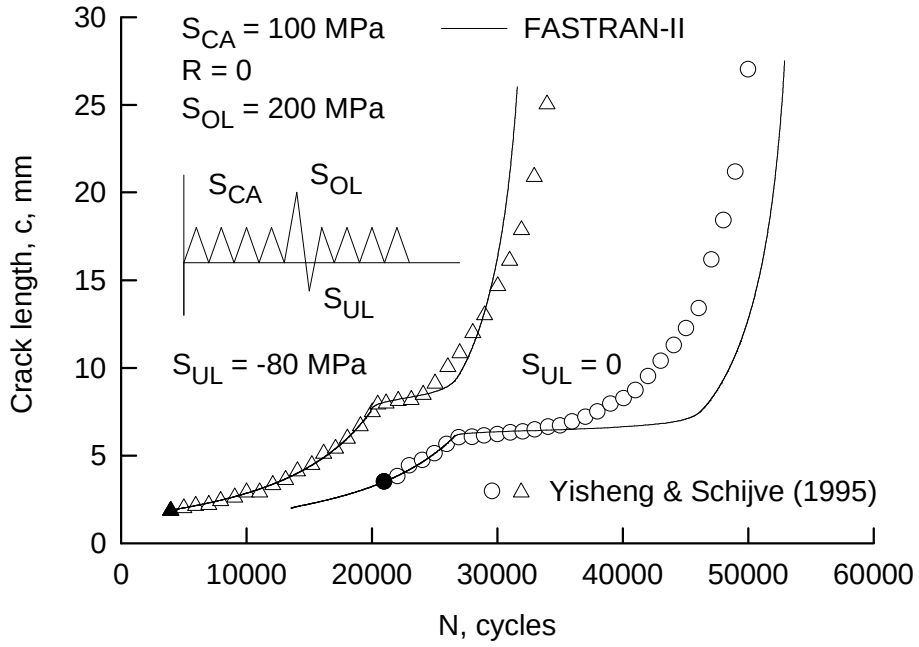

Figure 2 - Measured and calculated crack length against cycles during a single spike overload and underload.

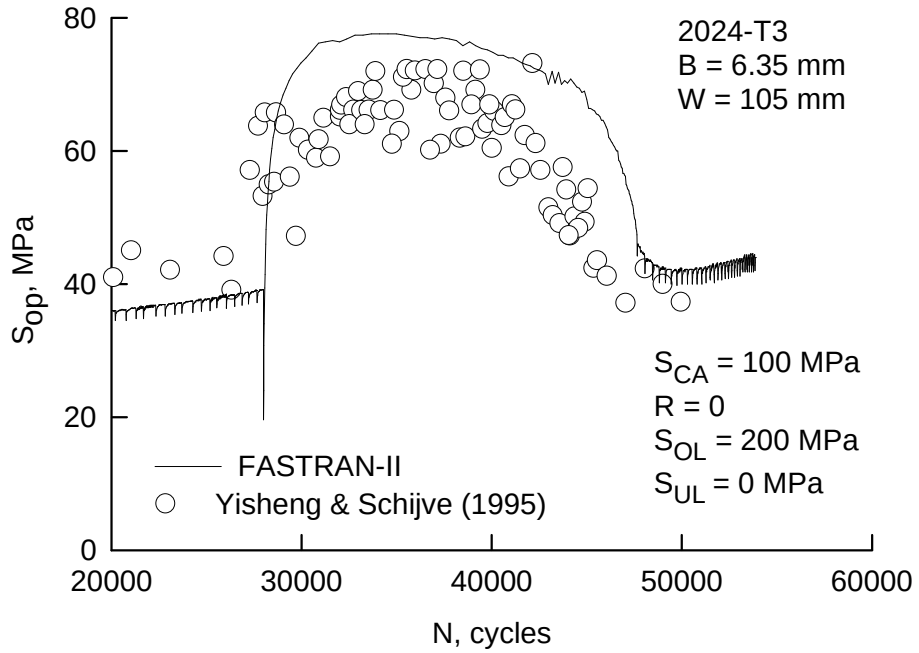

Figure 3 - Measured and calculated crack-opening stresses during a single spike overload.

REPEATED SPIKE OVERLOADS AND UNDERLOADS

Dawicke (1996) conducted repeated spike overloads and underloads tests on middle-crack tension specimens made of the 2.3 mm-thick aluminum alloy. All specimens (W = 76.2 mm) were fatigue precracked under constant-amplitude loading (S_{CA} = 70 MPa at R = 0.02) until a

12.7 mm crack was produced. Then a repeated spike overload/underload sequence was applied every 2500 cycles until failure. Overload ratios (S_{OL}/S_{CA}) ranged from 1.125 to 4, and underload ratios (S_{UL}/S_{CA}) ranged from 0 to -3. The number of cycles required to grow the crack from the initial size to failure was recorded.

The fatigue crack-growth lives, N_f (to grow a crack from 12.7 mm to failure), for various repeated spike overload magnitudes are shown in Figure 4 as symbols. The longest fatigue life occurred at an S_{OL}/S_{CA} ratio of 2. When the overload ratio reached 3.75, the specimen failed on the first application of the overload. The solid curve shows the predicted lives using the baseline relation shown in Figure 1 with the constraint-loss option. The predicted lives were generally within a factor of two of the test data. Comparing the fatigue surfaces for the constant-amplitude case and the small overload (S_{OL}/S_{CA} = 1.125) case, it became obvious that the small overload caused enough surface roughness to produce fretting-product-debris on the surface. The increased closure due to the debris was not included in the analysis. Thus, the model under predicted the fatigue lives for the small to moderate overloads. To illustrate why the constraint-loss regime is needed, predicted fatigue lives under a constant constraint factor of 2 are shown by the dashed curve. Here the predicted results can be as much as an order of magnitude in error.

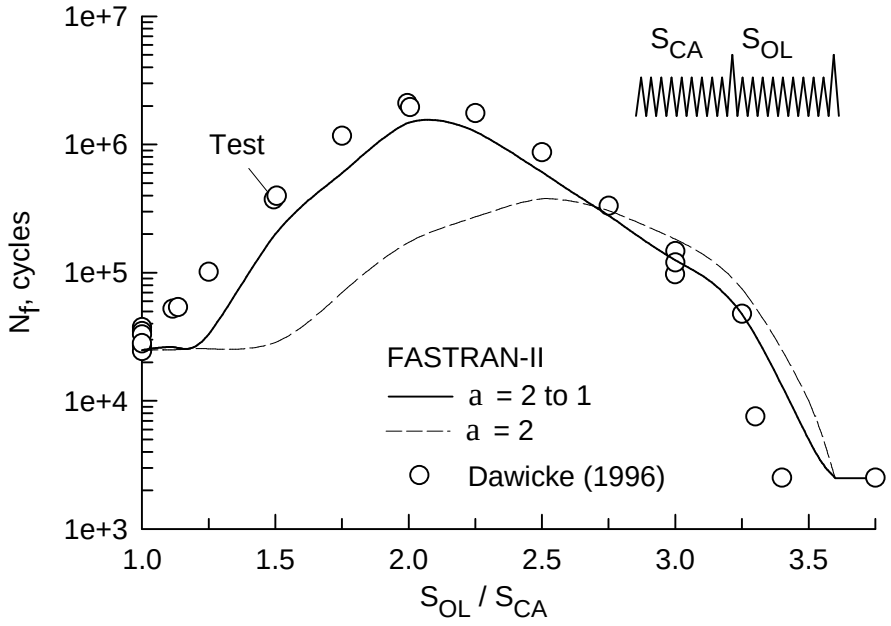

Figure 4 - Measured and predicted crack-growth lives for various repeated spike overloads.

AIRCRAFT SPECTRUM LOADING

Everett & Newman (unpubl.) conducted crack-growth tests under a commercial transport wing spectrum on middle-crack tension specimens made of the 2.3 mm-thick aluminum alloy. The wing spectrum had a flight schedule of 5000 flights with 5 different flights. The total number of cycles in a block of 5000 flights was about 208,000. Tests were conducted at maximum stress levels (S_{max}) in the spectrum of 138, 207 and 276 MPa. All specimens (W = 76.2 mm) were fatigue precracked under constant-amplitude loading (S_{CA} = 0.5 S_{max} at R = 0.05) until a 5 mm crack was produced. Then the wing spectrum loading was applied until failure.

Figure 5 shows measured and predicted crack length against cycles under the wing spectrum loading using the baseline relation and constraint values shown in Figure 1. Again,

Figure 5 shows why a constant constraint factor for "thin-sheet" alloys, $\alpha = 1$ or 2, will result in large differences between tests and analyses. Agreement between measured and predicted results for all three stress levels (207 and 276 MPa results are not shown) was well within ± 20 percent.

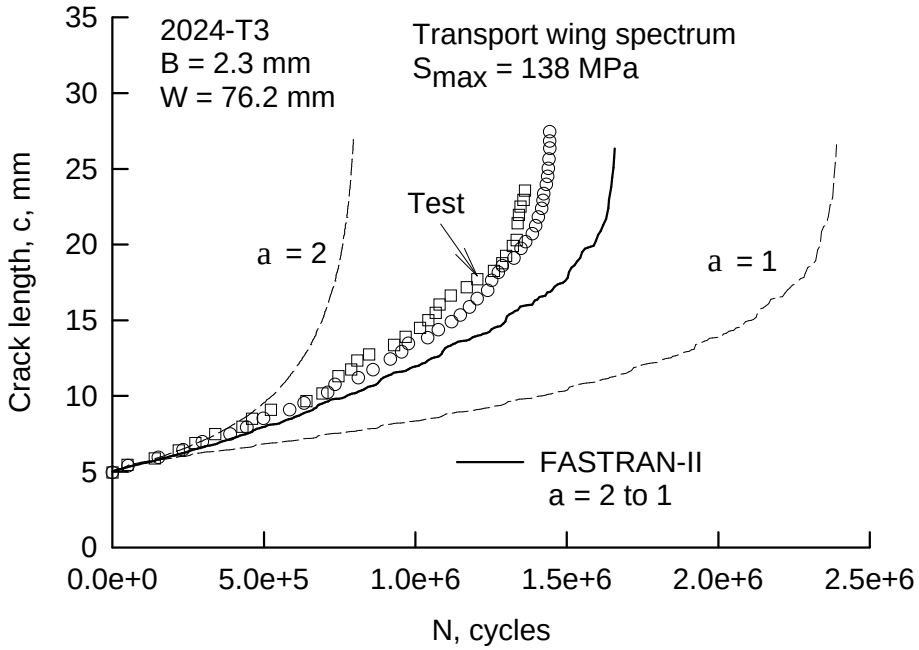

Figure 5 - Measured and predicted crack length against cycles for transport wing spectrum.

CONCLUDING REMARKS

A "plasticity-induced" crack-closure model was used to correlate crack-growth rate data on thin-sheet aluminum alloys under constant-amplitude loading for a wide range of stress ratios. A constraint factor, which accounts for three-dimensional state-of-stress effects, was used in determining the effective stress-intensity factor range against rate relations. A constraint-loss regime was selected to correspond to the flat-to-slant crack growth region. Comparisons made between measured and calculated crack length against cycles and crack-opening stresses under a single-spike overload and underload agreed quite well. Fatigue crack growth lives predicted under repeated spike overloads and underloads were generally within a factor of two of the test data. Predicted crack length against cycles for a commercial transport wing spectrum agreed within ± 20 percent of test data. Results shown indicated that the constraint-loss concept was needed to accurately predict crack growth under variable-amplitude loading in thin-sheet alloys.

ACKNOWLEDGEMENTS

The author takes this opportunity to thank Mr. E. P. Phillips, Dr. D. S. Dawicke, and Mr. R. A. Everett for their test results under constant-amplitude loading, repeated spike overloads, and aircraft spectrum loading, respectively, on the 2024-T3 aluminum alloy. Their test results were greatly appreciated and were very helpful in verifying the crack-closure model.

REFERENCES

Dawicke, D. S. 1996. Overload and underload effects on fatigue crack growth behavior of 2024-T3 aluminum alloy. NASA CR (in progress).

Dubensky, R. G. 1971. Fatigue crack propagation in 2024-T3 and 7075-T6 aluminum alloys at high stress. NASA CR-1732.

Dugdale, D. S. 1960. Yielding of steel sheets containing slits. *J. Mech. Phys. Solids* 8: 100-104.

Elber, W. 1971. The significance of fatigue crack closure. *Damage Tolerance in Aircraft Structures*. ASTM STP 486: 230-242.

Hudson, C. M. 1969. Effect of stress ratio on fatigue-crack growth in 7075-T6 and 2024-T3 aluminum alloy specimens. NASA TN D-5390.

Ling, M. R. & Schijve, J. 1988. Fractographic analysis of the crack growth rate and the shear lip development of 2024-T3 specimens under simple variable-amplitude loading. Delft University of Technology. Report LR-566.

Newman, J. C., Jr. 1976. Fracture analysis of various cracked configurations in sheet and plate materials. *Properties Related to Fracture Toughness*. ASTM STP 605: 104-123.

Newman, J. C., Jr. 1981. A crack-closure model for predicting fatigue crack growth under aircraft spectrum loading. *Methods and Models for Predicting Fatigue Crack Growth under Random Loading*. ASTM STP 748: 53-84.

Newman, J. C., Jr. 1983. A nonlinear fracture mechanics approach to the growth of small cracks. *Behaviour of Short Cracks in Airframe Components*. AGARD CP-328: 6.1-6.26.

Newman, J. C., Jr. 1984. A crack-opening stress equation for fatigue crack growth. *Int. J. Fracture*. 24: R131-R135.

Newman, J. C., Jr. & Edwards, P. R. 1988. *Short-crack growth behaviour in an aluminum alloy - an AGARD cooperative test programme*. AGARD R-732.

Newman, J. C., Jr. 1992a. FASTRAN II - a fatigue crack growth structural analysis program. NASA TM 104159.

Newman, J. C., Jr. 1992b. Effects of constraint on crack growth under aircraft spectrum loading. A. Beukers et al. (eds), *Fatigue of Aircraft Materials*. 83-109. Delft University Press.

Newman, J. C., Jr., Bigelow, C. & Shivakumar, K. 1993. Three-dimensional elastic-plastic finite-element analyses of constraint variations in cracked bodies. *Engng. Fract. Mech*. 46: 1-13.

Phillips, E. P. 1988. The influence of crack closure on fatigue crack growth thresholds in 2024-T3 aluminum alloy. *Mechanics of Fatigue Crack Closure*. ASTM STP 982: 505-515.

Schijve, J. 1967. Significance of fatigue cracks in micro-range and macro-range. *Fatigue Crack Propagation*. ASTM STP 415: 415-459.

Schijve, J. 1988. Fatigue crack closure observations and technical significance. J. C. Newman, Jr. & W. Elber (eds), *Mechanics of Fatigue Crack Closure*. ASTM STP 982: 5-34.

Vlasveld, J. A. & Schijve, J. 1980. Tongue-shaped crack extension during fatigue of high strength aluminum alloys. *Fat. Fract. Engng. Mat. Struct.* 3:129-145.

Yisheng, W. & Schijve, J. 1995. Fatigue crack closure measurements on 2024-T3 sheet specimens. *Fat. Fract. Engng. Mat. Struct*. 18: 917-921.